Available online at www.sciencedirect.com
SCIENCE DIRECT
Journal of Catalysis 230 (2005) 66–74
JOURNAL OF CATALYSIS
www.elsevier.com/locate/jcat

Deactivation of Au/CeO_x water gas shift catalysts

Chang Hwan Kim, Levi T. Thompson *

Department of Chemical Engineering, University of Michigan 2300 Hayward St., Ann Arbor, MI 48109, USA

Received 9 August 2004; revised 4 October 2004; accepted 6 October 2004

Available online 28 December 2004

Abstract

A series of CeO_2-supported gold catalysts were prepared and demonstrated to possess very high activities for the water gas shift reaction—a critical step in the production of H_2 for use in petroleum refining, chemicals synthesis, and proton exchange membrane fuel cells. While some of these catalysts were more active than a commercial Cu-based catalyst, they were susceptible to deactivation. Characterization using techniques including X-ray photoelectron and infrared spectroscopies indicated that the deactivation was caused primarily by blockage of the active sites by carbonates and/or formates. These species appeared to be formed by CO and H_2, and their formation was facilitated by oxygen deficient sites on ceria. The catalytic activity was fully recovered by calcination of the deactivated materials in flowing air at elevated temperatures. Details concerning the deactivation–regeneration behavior and microstructure of the Au/CeO_2 catalysts are discussed.

Keywords: Gold; Ceria; Water gas shift; Deactivation mechanism; Regeneration; Surface characterization; Microscopy

1. Introduction

The water gas shift (WGS) is a key reaction in the production of hydrogen for a number of processes, including petroleum refining and chemicals synthesis. An emerging application for the WGS is in the production of hydrogen for proton exchange membrane (PEM) fuel cells. This reaction is important because it removes CO, a poison to the fuel cell electrocatalysts, which is produced during the steam reforming and/or partial oxidation reactions. Copper- and Fe–Cr-based catalysts have been used commercially for the WGS; however, they are not suitable for portable and vehicular applications because of insufficient durabilities and activities. Consequently there is substantial interest in the development of better performing and more durable WGS catalysts [1–4].

Recently, Andreeva et al. [5,6] reported that gold catalysts supported on reducible oxides were highly active for the WGS reaction. Gold was thought to be relatively inactive [7,8] until Haruta reported that catalysts with Au particles smaller than 5 nm were highly active for CO oxidation [9,10]. The preferred technique for the preparation of highly dispersed Au-based catalysts is the deposition-precipitation method [6,9]. The high activity has most often been attributed to the loss of metallic character and an increase in the electronegativity or ionic character of the particles [11]. In fact, recently, based on results for a series of Au/CeO_2 catalysts from which most of the Au was leached, it was claimed that ionic Au was primarily responsible for the high WGS activity [12]. Conversely, Mohr et al. [13] reported that the active sites for CO hydrogenation were located on the edges of single crystalline gold particles. The high activities have also been linked to characteristics of the reducible oxide supports [14,15]. Titania and Co_3O_4 are reported to be good support materials for gold-based CO oxidation catalysts [9], and CeO_2 appears to produce the most active WGS catalysts [1,16].

For some reactions, supported gold catalysts have been reported to be susceptible to deactivation. There are several reports describing deactivation mechanisms for gold-based CO oxidation catalysts [17–20]. Kung et al. [17] observed the formation of carbonates during CO oxidation and pro-

* Corresponding author. Fax: 1-734-763-0459.
E-mail addresses: chkm@umich.edu (C.H. Kim), ltt@umich.edu (L.T. Thompson).

0021-9517/$ – see front matter
doi:10.1016/j.jcat.2004.10.004

posed a mechanism involving dehydroxylation of Au–OH. There are no reports regarding the deactivation of gold-based catalysts during WGS; however, ceria-supported Pt catalysts have been reported to be irreversibly overreduced by H_2 in the reformate [21].

In the present paper we report the preparation of Au/CeO_2 catalysts that are highly active for the WGS and their deactivation behavior in a simulated reformate mixture containing CO, H_2O, CO_2, H_2, and N_2. Characterization of the physical and chemical properties of the fresh and used catalysts helped define the deactivation mechanism. Finally, we also investigated the regenerability of the spent Au/CeO_2 catalysts.

2. Experimental

2.1. Catalyst preparation

The ceria was synthesized via the decomposition of cerium carbonate ($Ce_2(CO_3)_3 \cdot xH_2O$; Alfa Aesar) or used as received from Rhodia. The cerium carbonate was soaked in a mixture of 75% steam in N_2 at 150 °C then calcined in dry air at 400–700 °C for 4 h. These supports will be designated based on their calcination temperatures (e.g., CeO_2-400 was calcined at 400 °C). The ceria from Rhodia (CeO_2-RD) was also calcined in dry air at 400–700 °C for 4 h.

Catalysts designed to have loadings of 5 wt% Au were prepared by the deposition-precipitation method. The support material was thoroughly suspended in deionized water with stirring, and the temperature was held constant at 60 °C. A Na_2CO_3 solution (0.1 M) was added as necessary to maintain the pH at 10. An aqueous solution of $HAuCl_4 \cdot xH_2O$ (Alfa) was added dropwise to the suspended CeO_2 at a rate of 3 ml/min. The resulting precipitate material was aged for 30 min and then carefully washed with deionized water. The washed material was then dried under vacuum for 6 h.

The Au/CeO_2 powder was pelletized, crushed, and then sieved to limit the grain size to between 60 and 120 mesh (0.125–0.250 mm). A commercial WGS catalyst, Cu–Zn–Al (surface area of 60 m^2/g) obtained from Süd Chemie Ltd., was used to benchmark the Au/CeO_2 catalysts.

2.2. Catalyst characterization

Inductively coupled plasma optical emission spectroscopy (ICP-OES) was used to determine bulk compositions of the supported gold catalysts. The analysis was performed by Galbraith Laboratories, Inc. The surface areas (S_{BET}) and pore size distributions were determined with a Micromeritics ASAP 2010. All samples were degassed under vacuum at 200 °C until the static pressure was below 3 mm Hg. The instrumental error did not exceed 5%. X-ray diffraction (XRD) analysis was carried out with a Rigaku Rotaflex DMAX-B rotating anode X-ray diffractometer with a Cu-K_α radiation source operated at 40 kV and 100 mA. The transmission electron microscopic (TEM) analysis, including Z-contrast imaging and energy dispersive spectroscopy, was performed with a JEOL 2010F FEG source operating at 200 kV. High-resolution TEM was conducted with a JEOL 3011 UHR microscope operating at 300 kV. To achieve the appropriate electron transparency, the catalyst was crushed to a fine powder, and then a holey carbon film copper grid was dipped into the crushed powder. Particle size distributions were determined for more than 200 particles from several Z-contrast images from different areas of the samples.

X-ray photoelectron spectroscopy (XPS) was carried out with a Perkin–Elmer Phi ESCA 5400 spectrometer. Approximately 100 mg of powder was compressed into a wafer for analysis. Survey scans were used to identify constituents in the sample with binding energies between 0 and 1000 eV. The multiplex scans focused on the Au 4f, O 1s, and C 1s regions. These regions were scanned at a rate of 0.05 eV/s and cycled six times.

The Fourier transform infrared (FTIR) characterization was performed with a Thermo Electron Nexus 670 spectrometer equipped with an in situ diffuse reflectance (DRIFT) cell and a high-temperature environmental chamber. This chamber allowed simulation of the reaction conditions. The solid sample was diluted to 30 wt% with inert SiO_2 (Alfa, $S_{BET} \sim 5\ m^2/g$). The sample was reduced with a mixture of 5% H_2 in N_2 at 200 °C prior to analysis. After reduction, the sample was purged with either dry N_2 or air, and then the spectra were acquired. For some experiments, a mixture of 3% CO and 6% H_2 in N_2 was passed over the sample at 240 °C for 4 h to simulate conditions during catalyst deactivation.

Temperature-programmed oxidation (TPO) and CO chemisorption were performed with a Micromeritics AutoChem 2910 equipped with a Thermo Onix mass spectrometer. The samples were degassed in He at 200 °C prior to analysis. For TPO, the material was heated from room temperature to 400 °C in flowing air (20 cc/min), and the amounts of CO_2, CO, H_2O, and H_2 were monitored with the mass spectrometer. For the CO chemisorption experiments, calibrated volumes (5.1020 ml) of a 10% CO/He mixture were pulsed over the samples until the surface was saturated. The chemisorption experiments were carried out at 200 °C, a temperature that was similar to that used to determine the WGS rates. Prior to exposure of the catalyst to CO, the materials were pretreated at 200 °C in 5% H_2 in Ar.

2.3. Reaction rate measurements

An inert, low-surface-area SiO_2 (Alfa, $S_{BET} \sim 5\ m^2/g$) was used to dilute 15–30 mg of the catalyst to 50 wt%. The catalyst/SiO_2 mixture was loaded into a quartz microreactor and then reduced in a mixture of 4% H_2 in N_2 for 4 h prior to the activity measurements. The catalytic properties were measured at atmospheric pressure and temperatures ranging from 200 to 240 °C with a reactant gas whose composition was designed to simulate reformate from gasoline partial

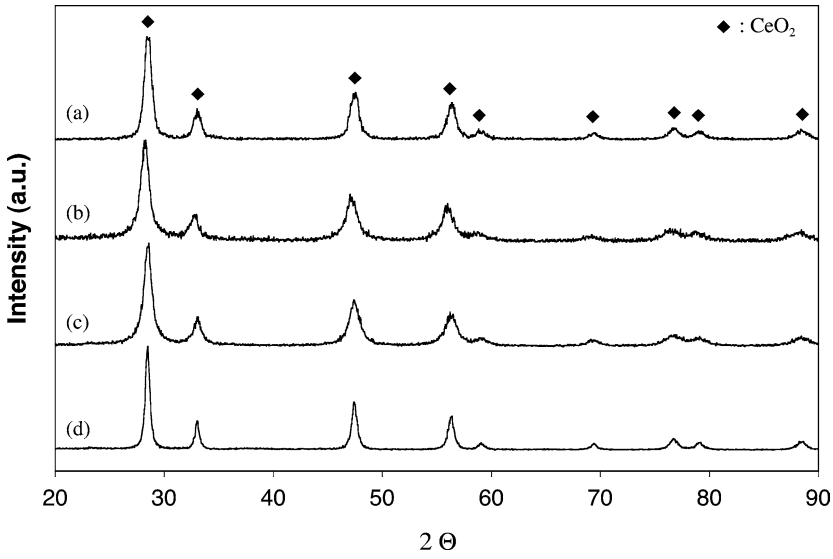

Fig. 1. X-ray diffraction patterns for (a) CeO_2-400, (b) Au/CeO_2-400, (c) Au/CeO_2-600, and (d) Au/CeO_2-700 catalysts.

Table 1
Microstructural properties for ceria supports

Sample	Calcination temperature (°C)	S_{BET} (m^2/g)	Cumulative pore volume (cm^3/g)	Average pore size (nm)
CeO_2-400	400	203	0.18	1.6
CeO_2-500	500	160	0.15	1.8
CeO_2-600	600	122	0.13	2.0
CeO_2-700	700	50	0.10	3.6
CeO_2-RD-400	400	155	0.12	1.5
CeO_2-RD-600	600	105	0.10	1.8
CeO_2-RD-700	700	38	0.08	3.6

Table 2
Surface areas and gold loadings for Au/CeO_2 catalysts

Sample	S_{BET} (m^2/g)	Au content (wt%)
Au/CeO_2-400	193	4.83
Au/CeO_2-500	148	4.56
Au/CeO_2-600	105	4.35
Au/CeO_2-700	45	3.30
Au/CeO_2-RD-400	140	4.79
Au/CeO_2-RD-600	88	4.44
Au/CeO_2-RD-700	35	2.54

oxidation. In particular, the CO, H_2O, CO_2, H_2, and N_2 concentrations were 10, 22, 6, 43, and 19 mol%, respectively. A high-performance liquid chromatography pump was used to add H_2O (0.04 ml/min liq.) to the reactant. The flow rates of each gas were controlled ussing mass flow controller, and the dry gases were mixed with H_2O in the vaporizer. The effluent was analyzed with a SRI 8610C gas chromatograph with a single Carboxen 1000 column.

3. Results and discussion

3.1. Microstructural properties

Surface areas for the ceria support materials are given in Table 1. For both the carbonate-derived and commercial ceria, the BET surface area decreased with increasing calcination temperature. Surface areas for the Au/CeO_2 catalysts were similar to those for the supports (Table 2). The measured gold loadings are also listed in Table 2; these were near 5%, the target loading, for materials calcined at 600 °C or less. It is not clear why loadings for materials calcined at 700 °C were lower than 5%, although surface areas for these materials were considerably lower than those for materials calcined at lower temperatures. Assuming atomic dispersion and 10^{15} atoms/cm^2, a loading of 2.5 wt% on a support with 35 m^2/g would correspond to a surface coverage of 22%.

X-ray diffraction patterns for the Au/CeO_2 catalysts did not reveal evidence of gold particles larger than ≈ 20 nm, the detection limit for the technique (see, for example, Fig. 1). High-resolution TEM images confirmed that the gold particles were smaller than about 10 nm (see, for example, Fig. 2). The peak in the particle size distribution was typically near 3 nm, as seen in Fig. 3, and the average particle size was approximately 5 nm.

3.2. Catalytic activity

Whereas CeO_2 was inactive for the WGS reaction, the Au/CeO_2 catalysts were initially very active, with rates that were in some cases superior to those for a commercial Cu–Zn–Al catalyst. WGS rates for the Au/CeO_2-400 and Cu–Zn–Al catalysts are plotted as a function of time on stream in Fig. 4 and summarized in Table 3. The other Au/CeO_2 catalysts behaved in a similar fashion. The initial rate for the Au/CeO_2-400 catalyst, the most active of the Au/CeO_2 catalysts, was almost four times higher than that of the Cu–Zn–Al catalyst; however, its activity decreased by more than 50% during the first 12 h on-stream. The deactivation trends

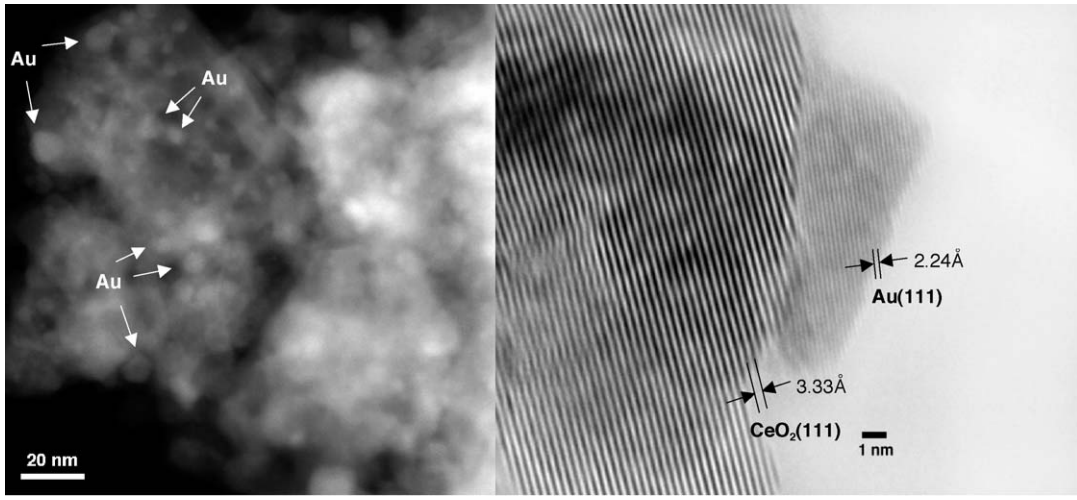

Fig. 2. Z-contrast (a) and high resolution (b) transmission electron micrographs for Au/CeO_2-400.

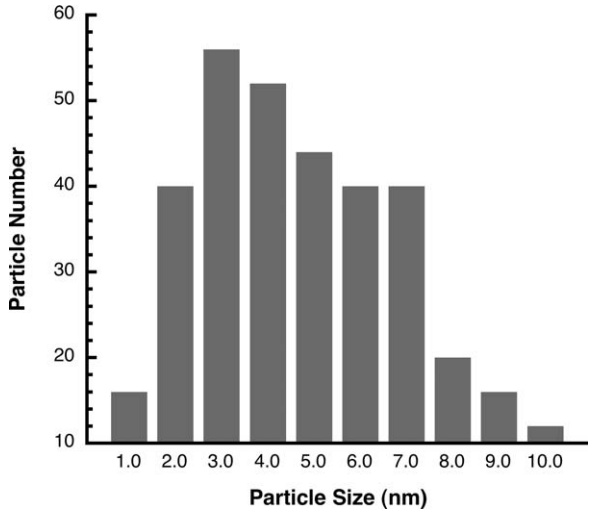

Fig. 3. Particle size distribution for Au/CeO_2-400.

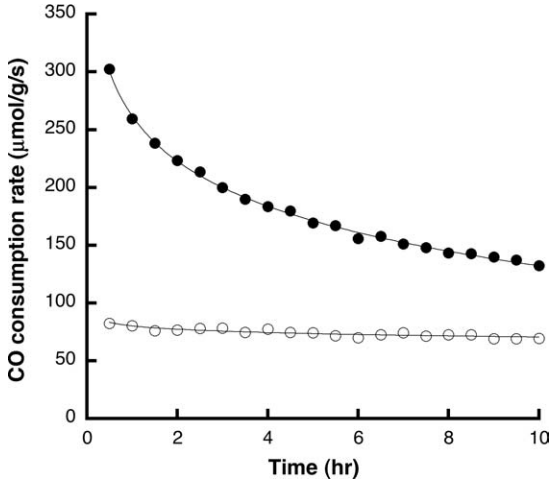

Fig. 4. Water gas shift rates at 240 °C as a function of time on stream for Au/CeO_2-400 (●) and Cu–Zn–Al (○) catalysts.

Table 3
Water gas shift rates at 240 °C for ceria, and the Au/CeO_2 and Cu–Zn–Al catalysts

Sample	S_{BET} (m^2/g)	Initial rate mmol/(g s)	Final rate mmol/(g s)
CeO_2-400	203	–	–
Au/CeO_2-400	193	293 ± 15	131 ± 10
Cu–Zn–Al	60	71 ± 8	60 ± 5

are consistent with fouling of the surface [22] but inconsistent with other reports in the literature regarding Au/CeO_2 WGS catalysts. In fact, we are not aware of any reports indicating that Au/CeO_2 catalysts deactivate during WGS [1,16]. Some evidence of deactivation has been reported for other types of reducible oxide-supported noble metal catalysts.

Zalc et al. recently attributed the deactivation of CeO_2-supported Pt catalysts during WGS to sintering or overreduction of the support by H_2 in the reformate [21]. Precious metals are known to catalyze the reduction of oxides by H_2 at relatively low temperatures [23]. Given the significant amounts of H_2 in the reformate, sintering or overreduction could be responsible for deactivation of the Au/CeO_2 catalysts.

During use in portable electronics and vehicular applications, the WGS catalysts will be subject to transients. To examine responses of the Au/CeO_x catalysts to transients, we carried out a series of experiments with the Au/CeO_2-400 catalyst in which the gas hourly space velocity (GHSV) was varied. Fig. 5 shows the CO conversion as a function of time on-stream with changing GHSV. Increasing the space velocity resulted in the anticipated decrease in the conversion but also aggravated the deactivation. When the space velocity was decreased to its initial value, the conversion did not recover completely. This suggests that transients may irreversibly deactivate the catalysts, a problem that plagues Cu–Zn–Al catalysts. In particular, cycling Cu–Zn–Al catalysts

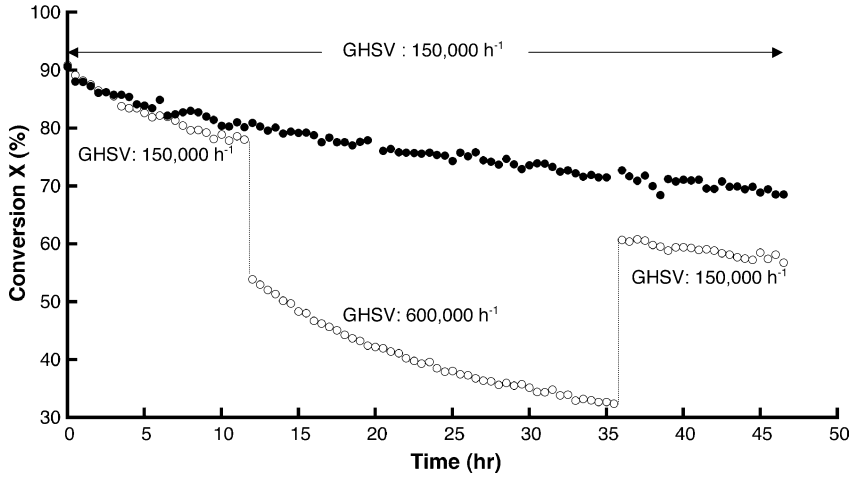

Fig. 5. Carbon monoxide conversion at 240 °C as a function of time on stream for the Au/CeO_2-400 catalyst at 150,000 h^{-1} (●), and space velocities of 150,000 and 600,000 h^{-1} (○).

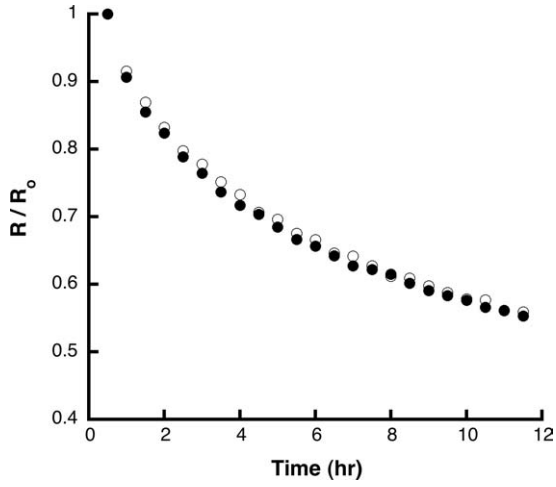

Fig. 6. Normalized WGS rates at 240 °C for the Au/CeO_2-RD-400 catalyst in the presence (●) and absence (○) of H_2.

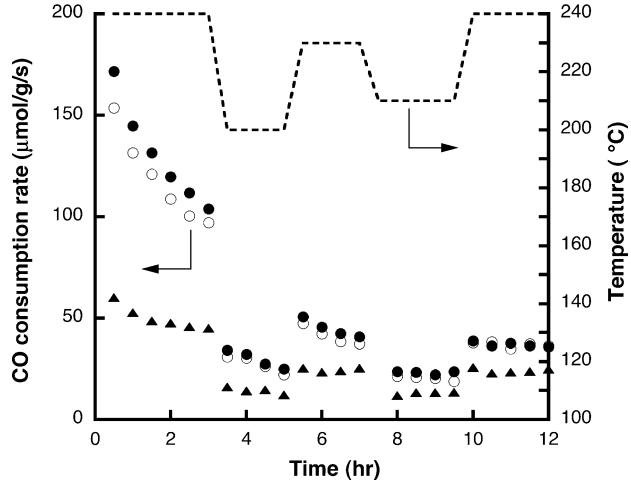

Fig. 7. Water gas shift rates for the Au/CeO_2-RD-400 catalyst following pretreatment in H_2 (●), CO (○), and a mixture of CO and H_2 (▲) at 240 °C for 6 h.

and exposing them to condensate causes severe, irreversible deactivation [24,25].

Variations in the deactivation behavior that occurred with changing conversion suggested that the CO and H_2 contents influenced the deactivation behavior. To assess the effect of H_2 on the deactivation behavior, He was substituted for H_2 in the reactant mixture (all other reaction conditions were the same). The results under these two conditions for the Au/CeO_2-RD-400 (Fig. 6) indicate that H_2 did not affect deactivation characteristics to any significant extent. In addition, there was no change in the surface area of the catalyst when it was used in WGS. Therefore, sintering and overreduction of the support were ruled out as causes for deactivation of the Au/CeO_x catalysts. Similar results have been reported for Pd-based catalysts by Wang et al. [26].

Carbon monoxide and H_2 in the reactant are likely sources for the formation of carbonaceous deposits including formates, carbonates, and/or carboxylates on the catalyst surface. To explore this possibility, the Au/CeO_2-RD-400 catalyst was pretreated with CO and H_2 separately, then with a mixture of H_2 and CO (20% each in N_2). The WGS rates following pretreatment are illustrated in Fig. 7. Separately, H_2 and CO did not affect the initial deactivation behavior, however, the catalyst was severely deactivated when pretreated with the H_2/CO mixture. This result implies that deactivation was caused by species formed by CO and H_2. Analysis using infrared and X-ray photoelectron spectroscopies was useful in characterizing these species.

3.3. Effect of support calcination temperature

Ceria is capable of existing in an oxygen-deficient state (CeO_{2-x} with $0 < x \leqslant 0.5$), even at temperatures less than 450 °C [27]. This oxygen deficiency has been reported to be an important factor with regard to the formation of carbonate and formate species on ceria. Li and co-workers, for example, reported that the formation of formates was due to the lack of sufficient surface oxygen [27–29]. In the presence of

Table 4
Initial and final water gas shift rates at 240 °C for various Au/CeO_2 catalysts

Sample	Initial rate (mmol/(g s))	Initial rate (mmol/(m^2 s))	TOF (s^{-1})	Final rate (mmol/(m^2 s))	$R_{final}/R_{initial}$
Au/CeO_2-400	293	1.5	0.7	0.53	0.35
Au/CeO_2-500	225	1.5	0.8	0.64	0.43
Au/CeO_2-600	158	1.5	1.5	0.76	0.51
Au/CeO_2-700	67	1.4	3.9	0.79	0.56
Au/CeO_2-RD-400	205	1.5	0.3	0.39	0.26
Au/CeO_2-RD-600	122	1.4	1.2	0.58	0.41
Au/CeO_2-RD-700	45	1.2	2.9	0.71	0.59

CO, CO_2, and H_2, they observed the formation of carbonate and formate species on the oxygen-deficient sites. The degree of oxygen deficiency can be adjusted through reduction of the materials, with the use of reductants like H_2 or CO, or through oxidation of the materials with the use of oxidants like O_2 and H_2O [30]. Therefore we compared the behavior of Au/CeO_x catalysts prepared using supports that were calcined at 400–700 °C in air. The surface area-normalized initial rates of all samples were very similar; these are given in Table 4. The implied result that the CeO_x support played an important role in the initial catalytic performance. Rates measured after 12 h on-stream did not correlate with the total surface area. Increasing the calcination temperature also caused a decrease in the surface area and an improvement in the degree of activity maintenance ($R_{final}/R_{initial}$). This implied that increasing the support calcination temperature decreased the potential for carbonate and/or formate deposition.

Turnover frequencies were estimated based on the initial rates and CO chemisorption uptake rates. Although there is no consensus regarding the appropriate chemisorbate for these types of catalyst, CO seemed to be a reasonable probe, given that it is a reactant [11]. The corresponding turnover frequencies ranged from 0.3 to nearly 4.0 s^{-1} at 240 °C. Unless there were multiple types of active sites, this result suggested that CO did not selectively characterize active sites on Au/CeO_x catalysts calcined at different temperatures.

3.4. Regeneration of the Au/CeO_2 catalysts

For many catalysts carbonaceous deposits can be removed, at least partially, via calcination in air or O_2. We used TPO to determine conditions that might remove the carbonaceous deposits. The signal for CO_2 production for the fresh and deactivated Au/CeO_2-RD-400 catalysts are illustrated in Fig. 8. The rate and amount of CO_2 produced were significantly higher for the deactivated catalyst. Most of the carbonaceous deposits reacted with oxygen at temperatures between 150 and 300 °C. The amount of CO_2 produced was equivalent to 1.17×10^{19} molecules/g. For a 5 wt% Au/CeO_2 catalyst, there would be 1.53×10^{20} Au atoms/g. Based on the Au particle size (5–10 nm) and the predominant shape (hemispherical), we estimated a dispersion of 15–30%. With this assumption, the ratio of CO_2 desorbed

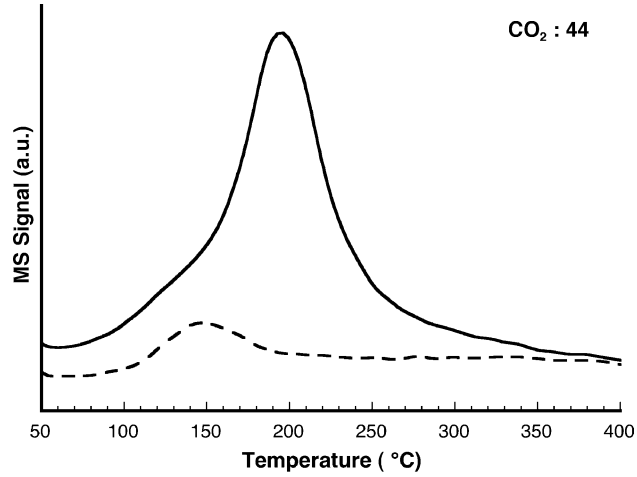

Fig. 8. Mass spectra for CO_2 desorbed during temperature-programmed oxidation from the deactivated (- - -), and fresh (—) Au/CeO_2-RD-400 catalyst.

to the number of Au atoms exposed on the surface was approximately 0.40. This value is similar to the relative activity loss during deactivation of the catalysts, implying that carbonaceous species blocked active sites for WGS.

Fig. 9(a) illustrates rates for the Au/CeO_2-RD-400 at four different temperatures. The deactivated catalyst was then calcined in flowing air at 400 °C for 4 h and reduced in a mixture of the 5% H_2 in N_2 (same as the pretreatment for fresh catalyst). More than 95% of its initial activity was recovered after the calcination treatment (Fig. 9(b)). This observation supports the conclusion that deactivation of the Au/CeO_x catalysts was due to surface fouling and not sintering of the Au or support, or irreversible overreduction of support.

3.5. Surface characterization of the deactivated catalyst

To better understand the cause of deactivation, surface properties of the Au/CeO_2-RD-400 catalyst were characterized. Carbon monoxide uptakes were measured prior to use in the WGS reaction, immediately after reaction, and immediately after the TPO experiment was carried out. The results are given in Table 5. The CO uptakes were proportional to the WGS rate, yielding turnover frequencies of 0.3 s^{-1} for all of the catalysts at 240 °C.

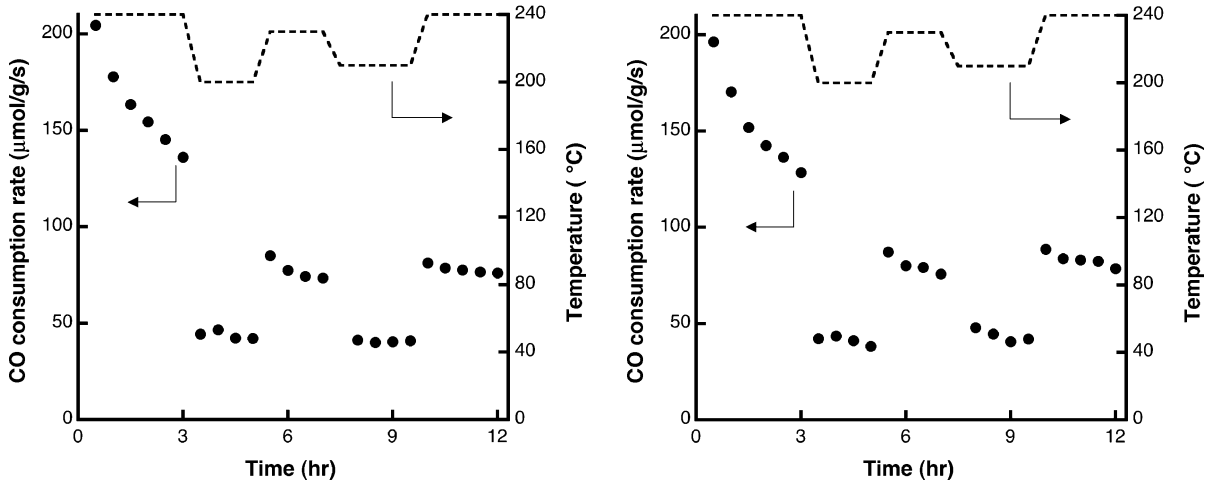

Fig. 9. Water gas shift rates for the (a) fresh Au/CeO_2-RD-400 catalyst and (b) deactivated Au/CeO_2-RD-400 catalyst following regeneration in dry air at 400 °C for 4 h.

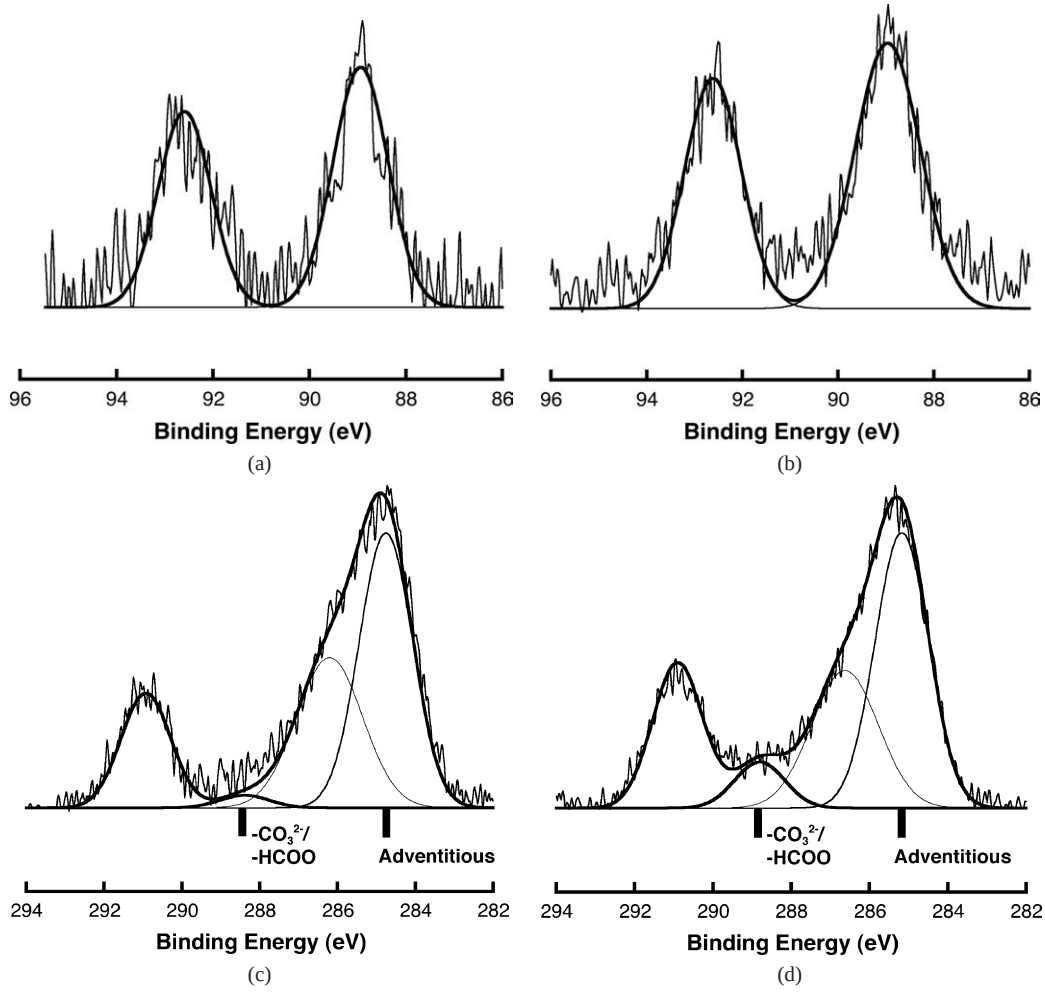

Fig. 10. X-ray photoelectron spectra in the Au 4f region for the (a) fresh and (b) deactivated Au/CeO_2-RD-400 catalyst, and in the C 1s region for the (c) fresh, and (d) deactivated catalyst.

X-ray photoelectron and FTIR spectroscopies were used to characterize chemical species on the fresh and deactivated catalysts. X-ray photoelectron spectra for the C 1s and Au 4f regions are shown in Fig. 10. Features in the Au 4f regions were nearly identical for the fresh and deactivated catalysts and indicated the presence of gold in a relatively high oxidation state. We should note that the deactivated catalyst was exposed to air prior to XPS analysis, so the surface may

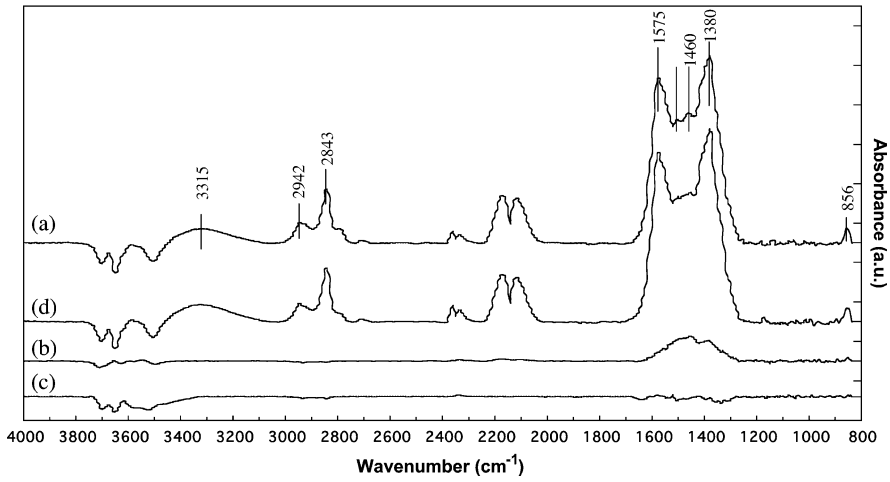

Fig. 11. Infrared spectra for the Au/CeO_2-RD-400 catalyst following treatment in (a) CO/H_2 mixture for 4 h at 240 °C, (b) air for 1 h at 240 °C, (c) air for 30 min. at 400 °C, and (d) re-exposure to CO/H_2 mixture for 1 h at 240 °C.

Table 5
Water gas shift rates at 240 °C and pulsed CO chemisorption uptakes at 200 °C for various catalysts

Sample	S_{BET} (m^2/g)	WGS rate (μmol/(g s))	CO uptake (ml/g)	TOF (s^{-1})
Au/CeO_2-RD-400 (fresh)	140	205	14.6	0.3
Au/CeO_2-RD-400 (deactivated)	145	55	2.8	0.4
Au/CeO_2-RD-400 (after TPO)	138	201	16.3	0.3
CeO_2-RD-400	155	–	0.4	–

have reoxidized, and impurities such as CO_2 may have adsorbed to the surface. Deconvolution of the C 1s spectra indicated that there were four different carbon species on the catalytic surface: adventitious carbon (285.1 eV), carbon associated with adsorbed CO_2 (290.1 eV), R–OH (286.4 eV), and –COOR:CO_3^{2-} (288.8 eV) [31]. When the fresh and deactivated catalysts were compared, the peak at 288.8 eV increased significantly. This was taken as evidence that both carbonate and formate species were formed during WGS over the Au/CeO_x catalysts.

Evidence for surface carbonates and formates was also observed in the FTIR spectra. Infrared spectra taken after exposure to various gases are shown in Fig. 11. Peaks located near 1300, 1500, 2800, and 2900 cm^{-1} correspond to formate species, and peaks at 1300 and 1400 cm^{-1} were likely due to the presence of carbonates [28,29]. Exposing the fresh catalyst to the mixture of CO and H_2 at 240 °C for 1 h caused a significant increase in the density of carbonates and formates. After calcination of this catalyst in air at 240 °C, most of the formate species were removed, but evidence of carbonates remained. Calcining the materials at 400 °C removed all of the adsorbed species produced during CO/H_2 exposure. This behavior was reproduced upon cycling of the materials through CO/H_2 exposure and calcinations, suggesting that the deposition of formate and carbonate was reversible.

4. Summary

Ceria-supported Au catalysts were prepared and evaluated for the WGS reaction. Initial activities for some of these catalysts were higher than those for a commercial Cu–Zn–Al catalyst, but the Au/CeO_2 catalysts were subject to deactivation. Results described in this paper indicate that deactivation was due to the formation of carbonates and/or formates on the catalyst surface. This conclusion is inconsistent with earlier reports that the deactivation of reducible oxide-supported noble metal catalysts was due to overreduction of the support and sintering. Initial activities for the Au/CeO_2 catalysts could be fully recovered by calcination of the deactivated catalysts in flowing air at elevated temperatures. We propose that the deposition of carbonates and/or formates was facilitated by oxygen-deficient sites on the catalyst surface. This implies that deactivation could be managed by conditioning of the CeO_2 surface or the addition of constituents to minimize oxygen deficiency.

References

[1] Q. Fu, A. Weber, M. Flytzani-Stephanopoulos, Catal. Lett. 77 (2001) 87.
[2] T. Bunluesin, R.J. Gorte, G.W. Graham, Appl. Catal. B 15 (1998) 107.
[3] J. Patt, D.J. Moon, C. Phillips, L. Thompson, Catal. Lett. 65 (2000) 193.
[4] T. Tabakova, V. Idakiev, D. Andreeva, I. Mitov, Appl. Catal. A 202 (2000) 91.
[5] D. Andreeva, V. Idakiev, T. Tabakova, A. Andreev, J. Catal. 158 (1996) 354.
[6] D. Andreeva, T. Tabakova, V. Idakiev, P. Christov, R. Giovanoli, Appl. Catal. A 169 (1998) 9.
[7] J. Schwank, Gold Bull. 18 (1985) 2.
[8] J. Schwank, Gold Bull. 16 (1983) 103.
[9] M. Haruta, S. Tsubota, T. Kobayashi, H. Kageyama, M.J. Genet, B. Delmon, J. Catal. 144 (1993) 175.

[10] M. Haruta, T. Kobayashi, H. Sano, N. Yamada, Chem. Lett. (1987) 405.
[11] G.C. Bond, D.T. Thompson, Catal. Rev. 41 (1999) 319.
[12] Q. Fu, H. Saltsburg, M. Flytzani-Stephanopoulos, Science 301 (2003) 935.
[13] C. Mohr, H. Hofmeister, J. Radnik, P. Claus, J. Amer. Chem. Soc. 125 (2003) 1905.
[14] M. Haruta, S. Tsubota, A. Ueda, H. Sakurai, Stud. Surf. Sci. Catal. 77 (1993) 45.
[15] M. Haruta, Catal. Today 36 (1997) 153.
[16] D. Andreeva, V. Idakiev, T. Tabakova, L. Ilieva, P. Falaras, A. Bourlinos, A. Travlos, Catal. Today 72 (2002) 51.
[17] C.K. Costello, M.C. Kung, H.S. Oh, Y. Wang, H.H. Kung, Appl. Catal. A 232 (2002) 159.
[18] Q.L. Guo, K. Luo, K.A. Davis, a D.W. Goodman, Surf. Interface Anal. 32 (2001) 161.
[19] G.Y. Wang, H.L. Lian, W.X. Zhang, D.Z. Jiang, T.H. Wu, Kinet. Catal. 43 (2002) 433.
[20] M. Valden, S. Pak, X. Lai, D.W. Goodman, Catal. Lett. 56 (1998) 7.
[21] J.M. Zalc, V. Sokolovskii, D.G. Loffler, J. Catal. 206 (2002) 169.
[22] R. Hughes (Ed.), Deactivation of Catalysts, Academic, London, 1984.
[23] C.N. Satterfield, in: Heterogeneous Catalysis in Industrial Practice, second ed., McGraw-Hill, New York, 1991.
[24] J.R. Ladebeck, J.P. Wagner (Eds.), Handbook of Fuel Cell Technology–Fundamentals, Technology, and Applications, Wiley, New York, 2003.
[25] M.W. Balakos, J.P. Wagner, in: 2002 Fuel Cell Seminar, Palm Springs, CA (November 2002), p. 18.
[26] X. Wang, R.J. Gorte, J.P. Wagner, J. Catal. 212 (2002) 225.
[27] A. Trovarelli, Catal. Rev. 38 (1996) 439.
[28] C. Li, Y. Sakata, T. Arai, K. Domen, K.I. Maruya, T. Onishi, J. Chem. Soc. Faraday Trans. 1 85 (1989) 1451.
[29] C. Li, Y. Sakata, T. Arai, K. Domen, K. Maruya, T. Onishi, J. Chem. Soc. Faraday Trans. 1 85 (1989) 929.
[30] A. Laachir, V. Perrichon, A. Badri, J. Lamotte, E. Catherine, J.C. Lavalley, J. Elfallah, L. Hilaire, F. Lenormand, E. Quemere, G.N. Sauvion, O. Touret, J. Chem. Soc. Faraday Trans. 87 (1991) 1601.
[31] V.I. Nefedov, in: X-Ray Photoelectron Spectroscopy of Solid Surfaces, first English ed., VSP, Utrecht, 1988.